Title
Analytical modelling and x-ray imaging of oscillations of a single magnetic domain wall

Permalink
https://escholarship.org/uc/item/6gt9v3s6

Author
Bocklage, Lars

Publication Date
2009-09-20

Peer reviewed

Analytical Modelling and X-Ray Imaging of Oscillations of a Single Magnetic Domain Wall

Lars Bocklage,[1,*] Benjamin Krüger,[2,†] Peter Fischer,[3] and Guido Meier[1]

[1]*Institut für Angewandte Physik und Zentrum für Mikrostrukturforschung, Universität Hamburg, Jungiusstrasse 11, 20355 Hamburg*

[2]*I. Institut für Theoretische Physik, Universität Hamburg, Jungiusstrasse 9, 20355 Hamburg*

[3]*Center for X-Ray Optics, Lawrence Berkeley National Laboratory, 1 Cyclotron Road, Berkeley, CA 94720, USA*

(Dated: May 6, 2009)

Abstract

Domain-wall oscillation in a pinnig potential is described analytically in a one dimensional model for the field-driven case. For a proper description the pinning potential has to be extended by nonharmonic contributions. Oscillations of a domain wall are observed on its genuine time scale by magnetic X-ray microscopy. It is shown that the nonharmonic terms are present in real samples with a strong restoring potential. In the framework of our model we gain deep insight into the domain-wall motion by looking at different phase spaces. The corrections of the harmonic potential can change the motion of the domain wall significantly. The damping parameter of permalloy is determined via the direct imaging technique.

PACS numbers: 68.37.Yz,75.60.Ch,76.50.+g,85.75.-d

*Electronic address: `lbocklag@physnet.uni-hamburg.de`
†Electronic address: `bkrueger@physnet.uni-hamburg.de`

I. INTRODUCTION

Fast magnetization dynamics on the micro- and nanometer scale are an intersting field of research because magnetization patterns with single elementary magnetic structures, like vortices or domain walls, form on these fundamental magnetic lengthscales. Their dynamics occur on the nano- and picosecond time scale. Both size and speed of these patterns are of great interest in todays research for prospective non-volatile data storage devices [1–3]. Although these magnetization structures are coupled locally via the exchange interaction and globally via the magnetic stray field an analytical description of their dynamics is possible [4, 5]. The motion of the magnetization can be excited by field or current and both and can be included in the analytical description [6, 7]. If the motion of a domain wall along a nanowire is caused by current or by field is unambiguously determinable [8–10]. However, the distinction of these effects is not simple [11–13], as the current is always accompanied by its magnetic Oersted field. In the case of vortices or domain walls in confining potentials the identification of the driving force is even more complicated. Spatially and temporally resolved experimental methods are needed. One possible tool is magnetic transmission X-ray microscopy (MTXM), which provides a spatial resolution down to 15 nm [14] and a temporal resolution below 100 ps [15]. This method matches the requirements to study magnetization dynamics on fundamental scales.

In this work we study the dynamics of a confined magnetic domain wall. It is organized as follows. After the introduction we focus in the second part on the analytical description of field-induced oscillations of a single domain wall. An analytical solution of the Landau-Lifshitz-Gilbert equation is deduced. In the third section the experimental setup used to image domain-wall oscillations is described. In the fourth part we present results of time resolved X-ray microscopy and its analytical description. We show that a simple harmonic oscillator model can not describe the dynamics of the wall. Higher-order terms are required to describe the confining potential of the domain wall in the experiments. The damping parameter of permalloy has been intensively studied with ferromagnetic resonance or with Kerr microscopy [16–21]. Here we determine the damping parameter with a direct imaging technique capable to observe the motion of the magnetization on its genuine time- and lengthscale. Section five ends with a conclusion.

II. MICROMAGNETIC MODEL

The Landau-Lifshitz-Gilbert (LLG) equation

$$\frac{d\vec{M}}{dt} = -\gamma\vec{M}\times\vec{H}_{\text{eff}} + \frac{\alpha}{M_S}\vec{M}\times\frac{d\vec{M}}{dt}\ . \tag{1}$$

describes the dynamics of the magnetization $\vec{M}$. $\vec{H}_{\text{eff}}$, γ, α, and M_S are the effective magnetic f eld, the gyromagnetic ratio, the Gilbert damping parameter, and the saturation magnetization, respectively. The domain-wall dynamics are implicated by the LLG-equation and can be described analytically with the assumption of a rigid domain wall [22]. The equations of motion have been derived in Ref. [6]. We neglect the current-induced terms of the dynamics and obtain the equations of motion for the center of the wall Y and the angle of the rotation of the wall out-of-plane ϕ

$$\dot{Y} = -\frac{2\lambda\gamma' K_\perp}{\mu_0 M_S}\phi - \lambda\gamma'\alpha H(Y) \tag{2}$$

and

$$\dot{\phi} = \gamma' H(Y) - \frac{2\gamma'\alpha K_\perp}{\mu_0 M_S}\phi\ , \tag{3}$$

with $\gamma' = \gamma/(1+\alpha^2)$ and the domain wall width $\lambda = \sqrt{A/K}$. A is the exchange constant and K is the anisotropy constant for the magnetization pointing in the y-direction, while $K + K_\perp$ is the anisotropy for the magnetization pointing out-of-plane. The magnetic f eld H consists of the external f eld H_{ext}, which points perpendicular to the current, and the pinning f eld H_{pin}. In the time derivative of Eq. (2) $\dot{\phi}$ is replaced by the right-hand side of Eq. (3) which yields

$$\ddot{Y} = -\frac{2\lambda\gamma'^2 K_\perp}{\mu_0 M_S}\left(H(Y) - \frac{2\alpha K_\perp}{\mu_0 M_S}\phi\right) - \lambda\gamma'\alpha\dot{H}(Y)\ . \tag{4}$$

Solving Eq. (2) for the angle

$$\phi = -\frac{\mu_0 M_S}{2K_\perp}\left(\frac{1}{\gamma'\lambda}\dot{Y} + \alpha H(Y)\right) \tag{5}$$

and inserting this expression in Eq. (4), yields the following relation for the position of the DW

$$\ddot{Y} = -\frac{\lambda\gamma H(Y) + \alpha\dot{Y}}{\alpha\tau_d} - \lambda\gamma'\alpha\dot{H}(Y)\ . \tag{6}$$

The damping time τ_d is given by

$$\tau_d = \frac{\mu_0 M_S}{2\gamma'\alpha K_\perp}\ . \tag{7}$$

To derive the pinning field we solve the energy functional

$$E = \int \left[\frac{2K}{\cosh^2\left(\frac{y-Y}{\lambda}\right)} + \frac{A}{\cosh^2\left(\frac{y-Y}{\lambda}\right)} \left(\frac{\partial \phi}{\partial y} \right)^2 \right] dV + \int \left[\frac{K_\perp \phi^2}{\cosh^2\left(\frac{y-Y}{\lambda}\right)} - \mu_0 M_s H(Y) \tanh\left(\frac{y-Y}{\lambda} \right) \right] dV \tag{8}$$

given in Ref. [6]. The corresponding coordinate system is shown in Fig. 1. We neglect all constant contributions. The energy of the domain wall is then given by

$$E = 2S\lambda K_\perp \phi^2 + 2S\mu_0 M_s Y H(Y) \tag{9}$$

with the cross section S of the structure. As the field is $H(Y) = H_{\text{ext}}(Y) + H_{\text{pin}}(Y)$ one can seperate these parts. The pinning field is given by

$$H_{\text{pin}} = \frac{1}{2S\mu_0 M_s} \frac{dE_{\text{pin}}}{dY} \;, \tag{10}$$

For the reaction of the domain wall on the pinning field we get

$$\ddot{Y}_{\text{pin}} = \frac{\lambda \gamma'^2 K_\perp (1+\alpha^2)}{S\mu_0^2 M_s^2} \frac{dE_{\text{pin}}}{dY} = -\frac{1+\alpha^2}{m} \frac{dE_{\text{pin}}}{dY} \;. \tag{11}$$

The domain-wall mass m is defined in Ref. [6]

$$m = \frac{S\mu_0^2 M_s^2}{\lambda \gamma'^2 K_\perp} = \frac{2\alpha S \mu_0 M_s \tau_d}{\lambda \gamma'} \;. \tag{12}$$

With this definition of the mass the kinetic energy of the wall $\frac{1}{2} m\dot{Y}$ can be calculated for a stationary motion without magnetic fields. Interestingly the mass of the domain wall differs by a factor of $(1+\alpha^2)^{-1}$ to satisfy the equations of motion. Consequently a different mass $m' = \frac{m}{1+\alpha^2}$ determines the reaction of the wall on magnetic fields. As the damping parameter in permalloy is small the difference is negligible. However, in strongly damped systems this effect should be more pronounced. Eq. (6) becomes

$$\ddot{Y} = -\frac{\lambda \gamma H_{\text{ext}} + \alpha \dot{Y}}{\alpha \tau_d} - \lambda \gamma' \alpha \dot{H}_{\text{ext}} - \frac{1}{m'} \frac{dE_{\text{pin}}}{dY} \;. \tag{13}$$

The time derivative of the pinning field is small and can be neglected. In addition to the exciting field, the material parameters and the shape of the sample the dynamics of the domain wall also depend linearly on the width of the wall itself. The energy of the domain wall is given by

$$E = 2S\lambda K_\perp \phi^2 + 2S\mu_0 M_s Y H_{\text{ext}} + E_{\text{pin}} \;. \tag{14}$$

Oscillations of a single domain wall are characterized by the confining potential $E_{\rm pin}$. In a first approximation a harmonic potential

$$E_{\rm pin} = \frac{1}{2} m' \omega_{\rm r}^2 Y^2 \tag{15}$$

with the resonance frequency $\omega_{\rm r}$ is used to describe these oscillations. However, deviations from the harmonic potential can occur in a real sample depending on its size and shape [12, 23]. In this case nonharmonic terms have to be added to the potential which can be evolved into the power series

$$E_{\rm pin} = \sum_{n=1}^{\infty} \frac{1}{2n} m' k_n Y^{2n}. \tag{16}$$

Here $k_1 = \omega_{\rm r}^2$ and all constants of the higher order terms should be small compared to k_1. That these deviations occur and at least the first correction terms to the harmonic potential can be significant in real samples is shown by time-resolved imaging of the oscillations of a single domain wall described in Sec. IV.

In the following part of this section we show how the damping parameter can be calculated from the damping time and the domain-wall width. The anisotropy in y direction can be calculated from the domain-wall width as

$$K = \frac{A}{\lambda^2}. \tag{17}$$

The sum of all three magnetic anisotropy constants is given by

$$K_x + K_y + K_z = 2K + K_\perp = \frac{1}{2} \mu_0 M_s^2. \tag{18}$$

Insertion of Eq. (17) in Eq. (18) yields the value of the perpendicular anisotropy

$$K_\perp = \frac{1}{2} \mu_0 M_s^2 - 2 \frac{A}{\lambda^2}. \tag{19}$$

Inserting this result in Eq. (7) allows the determination of the damping parameter

$$\begin{aligned} \alpha &= x - \sqrt{x-1} \\ \text{with } x &= \tfrac{\gamma \tau_d (\mu_0 M_s^2 - 4A/\lambda^2)}{2 \mu_0 M_s} \end{aligned} \tag{20}$$

Apart from the known values of the saturation magnetization, the gyromagnetic ratio, and the exchange constant the damping time and the domain-wall width must be determined. Both are directly determined from the experimental data.

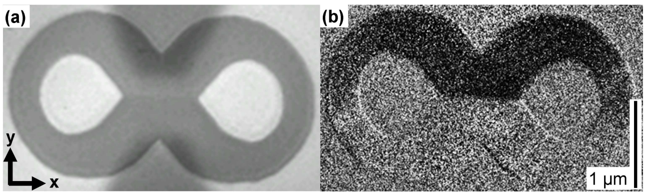

FIG. 1: (a) X-ray image of the investigated sample showing the permalloy structure and the gold contacts. (b) Static differential image obtained from an image at remanence and an image at saturation. It shows the altered magnetization in the upper part of the structure at remanence (black) in contrast to the saturated state. Therefore the magnetization of the black part has reversed and a 180° domain wall has formed at the intersection in the center.

III. EXPERIMENTAL SETUP

Time resolved X-ray microscopy is performed at beamline 6.1.2 at the Advanced Light Source in Berkeley, CA. This full-f eld soft X-ray transmission microscope provides magnetic contrast by the X-ray magnetic circular dichroism (XMCD) [24]. In the present measurements a spatial resolution of 25 nm is achieved by Fresnel zone plates. A stroboscopic pump-and-probe measurement scheme provides a temporal resolution below 100 ps [12]. Due to the transmission design of the microscope the microstructures have to be prepared on 100 nm thick Si_3N_4 membranes. Electron-beam lithography, thermal evaporation, and lift-off processing techniques are used to prepare the 20 nm thick permalloy ($Ni_{80}Fe_{20}$) structure shown in Fig. 1(a). The structure is contacted by wave guides fabricated by electron-beam lithography, DC-magnetron sputtering of 2 nm Al and 20 nm Au, and lift-off processing.

To identify the magnetic contrast X-ray images are illuminated at a saturated state and at remanence. The images are then divided and one obtains a grayscale image where the changed magnetization to the saturated state is indicated by white or black contrast (see Fig. 1(b)). The time resolved images are normalized to an image without excitation, i.e. without dynamics, which is typically the f rst image in a time scan ($t = 0$). Hereby the change of the magnetization at times $t > 0$ is detected by a changing contrast. We used steps of 200 ps to scan 6 ns time delay alltogether.

IV. RESULTS

Fig. 1(a) shows the investigated "infinity" shaped structure. The structure is saturated along the x-direction in a field of ∼50 mT. Afterwards the field is set to zero. Its magnetic contrast is shown in Fig. 1(b). The upper and lower part are magnetized inverse and a 180° domain wall is located at the intersection. The tip-shaped holes of the structure are pinning sites for the domain wall by minimizing the domain-wall length and energy. Therefore the domain wall is confined in a restoring potential.

The domain wall is excited by current pulses through the ferromagnetic structure. The current density is $5{\cdot}10^{11}$ A/m^2. The current flows directly through the structure in contrast to experiments where an Oersted field of a strip line is used as a source for radio frequency field excitation. Nonetheless, in the present experiments the main source of excitation is not spin-torque but the current's Oersted field. The exciting force is discussed in detail in Ref. [12]. The important point for the present study is that a short magnetic field pulse in x-direction excites the domain-wall oscillation. The field pulse has the same time structure as the current pulse.

Dynamic differential images are shown in Fig. 2(a) for different time steps. The field pulse length was 1.1 ns. The white and black contrast indicates a motion of the domain wall. Fig. 2(b) shows the progress of the maximal vertical deflection of the domain wall in y-direction for different pulse lengths. The domain wall is deflected as long as the current pulse is applied and oscillates around the deflected position. Afterwards the domain wall performs a free damped oscillation. To extract the potential of the domain wall the free oscillation is fitted to

$$y(t) = Ae^{-\Gamma(t-t_0)} \cos \omega(t - t_0) \tag{21}$$

for the current pulses of 1.1 ns duration. The fit is shown in Fig. 2 as dashed green line. The following parameters are obtained from the fit: the amplitude $A = 125$ nm, the damping constant $\Gamma = 554$ MHz, the start time of the free oscillation $t_0 = 1.85$ ns, and the free angular frequency $\omega = 3.6$ GHz. The free frequency f is 573 MHz and the damping time $\tau_d = (2\Gamma)^{-1}$ is 0.9 ns. The resonance frequency is given by $\omega_\mathrm{r} = \sqrt{\omega^2 + \Gamma^2}$. This simple model is adequate as long as the deflection of the domain wall is small and the restoring force is determined by a harmonic potential. We will see that the harmonic part of the total potential is well described with these parameters.

With Eq. (13) the entire time evolution of the domain-wall position can be fitted. The domain-wall position is calculated by a time integration of Eq. (13) using the explicit Euler method [25].

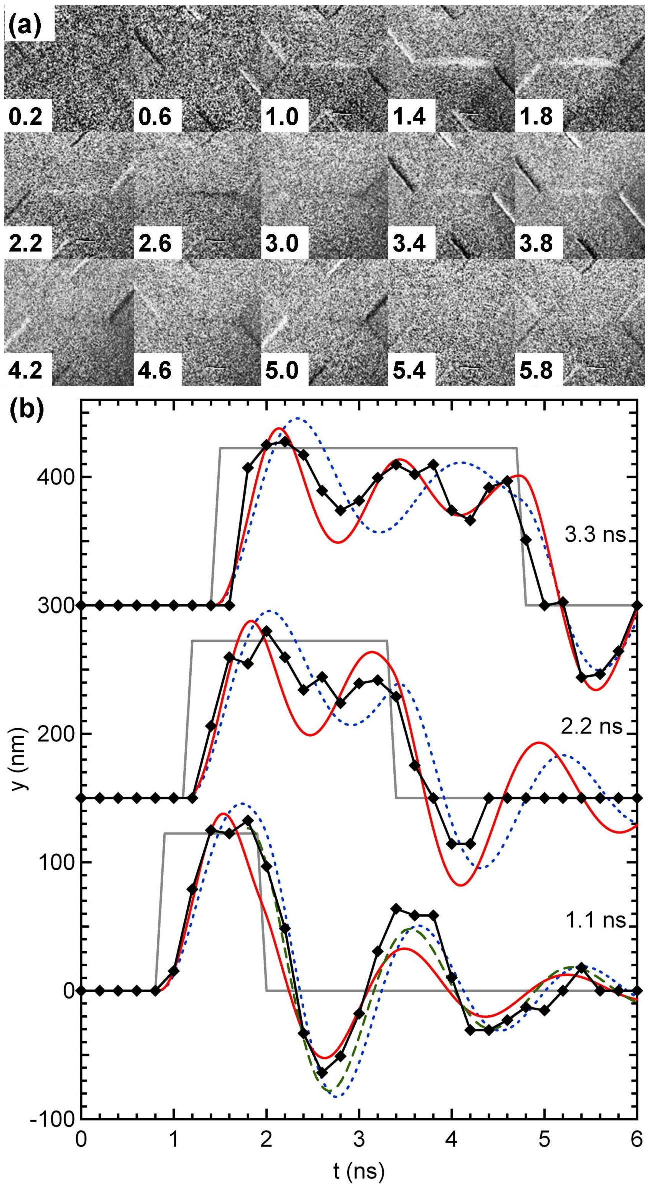

FIG. 2: (Color online) (a) Dynamic differential images for the inner section of the structure for different time steps indicated by the lower left number in units of nanoseconds. The pulse length is 1.1 ns. (b) Progress of the maximal vertical def ection of the domain wall (diamonds) for pulse lengths of 1.1 ns, 2.2 ns, and 3.3 ns. The curve offset for 2.2 ns (3.3 ns) is 150 nm (300 nm) for clarity. The black lines are guides to the eye. The grey lines depict the time structure of the current pulses. The dashed green curve is a f t to the free damped oscillation using Eq. (21) for a pulse width of 1.1 ns . The dotted blue and solid red lines are f ts to the integration of Eq. 13 with a harmonic and a nonharmonic potential, respectively.

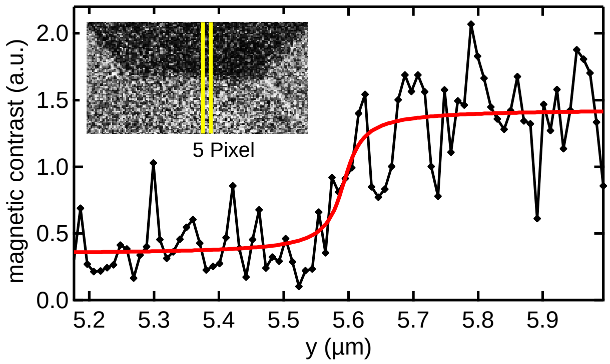

FIG. 3: (Color online) Contrast along the y-direction of the section shown in the inset. The value is averaged over 5 pixel along the x-direction. The red line is the wall angle θ fitted with Eq. (22).

Figure 2 shows fits for a harmonic potential and for a nonharmonic potential with fourth-order correction. One can see that the pure harmonic model can not describe the dynamics for increasing pulse lengths. This is due to the change in frequency for higher deflections by a stronger restoring force. The fit with the first nonharmonic correction is in good agreement with the experimental data. The fit parameter for the harmonic potential is $\mu_0 H_{\text{ext}} \lambda = -6.0 \cdot 10^{-11}$ Tm an the fit parameters for the nonharmonic potential are $\mu_0 H_{\text{ext}} \lambda = -7.5 \cdot 10^{-11}$ Tm and $k_2 = 4.5 \cdot 10^{-4}$ (ns)$^{-2}$(nm)$^{-2}$. With this magnitude of the nonharmonic term the harmonic potential holds well for deflections up to 70 nm. Therefore the frequency and the damping from the harmonic fit hold true.

The domain-wall width $\lambda = 23$ nm, the domain-wall mass $m = 7.6 \cdot 10^{-23}$ kg, and the exciting Oersted field $\mu_0 H_{\text{ext}} = -3.3$ mT are determined in Ref. [12]. The domain wall width was determined by using the field dependent deflection of the domain wall. This determination used the potential where we assumed $\alpha = 0.01$. To avoid this assumption in the determination of the damping parameter with Eq. (20) we use the direct imaging of the domain wall to get the wall width. Figure 3 shows the change in contrast depending on the y-direction averaged over five pixels in x-direction. The inset shows the analyzed area enclosed by yellow lines. The Néel wall angle

$$\theta = \pi - 2 \arctan(e^{(y-Y)/\lambda}) \tag{22}$$

is fitted to the change in contrast. We obtain a wall width of $\lambda = 22.1$ nm. This value is in the order of the resolution of the zone plates used in the experiments. By inserting the result for the domain-wall width λ in Eq. (20) we obtain a value of $\alpha = 0.0066$. For long domain walls, like the

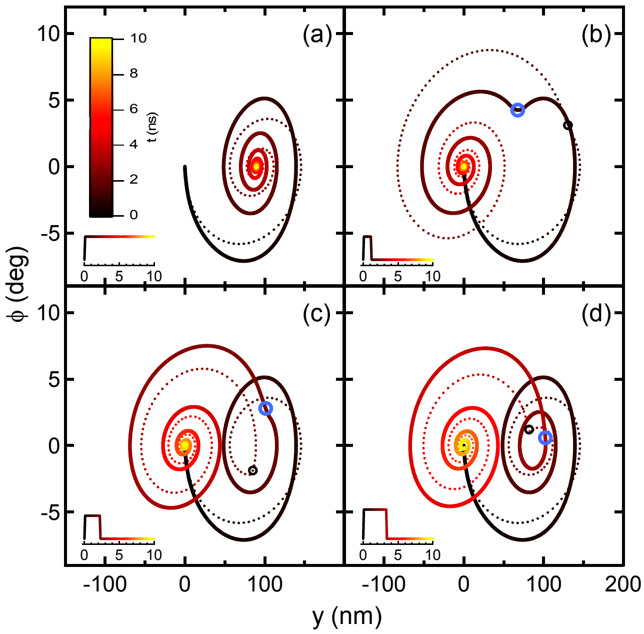

FIG. 4: (Color online) Trajectories in the phase space of position Y and out-of-plain angle ϕ of the domain wall for a step like f eld (a) and f eld pulses of 1.1 ns (b), 2.2 ns (c), and 3.3 ns (d). Trajectories for the harmonic and the nonharmonic potential are the dotted and the solid lines, respectively. The color scale indicates the time after the pulse start. The black and blue circles depict the time when the magnetic f eld has decreased to half of the amplitudefor the harmonic and nonharmonic potential, respectively. The insets depict the pulse prof le for the f rst 10 ns.

one observed in the experiment, the width is not necessarily constant. Therefore the width does not necessarily ref ect the width which has to be used to calculate the anisotropy. However the contribution of $4A/\lambda^2$ in Eq. (20) is small compared the the factor $\mu_0 M_s^2$. In addition we performed ferromagnetic resonance measurements on permalloy f lms using a broadband ferromagnetic resonance setup [26] and obtain a damping parameter of $\alpha = 0.0064$ in excellent agreement with the above value determined independently via direct imaging of the domain-wall oscillation. The values of the damping parameter α are also in good agreement with previous results [16–21].

A deeper insight in the domain-wall oscillation can be gained by visualizing the motion of the domain wall in various phase spaces. With Eq. (5) we calculate the angle ϕ for our three pulse lengths and for a step like function with the same slope as the f eld pulses in the experiment for both the harmonic and the non-harmonic potential derived from the f t. The trajectory in the phase space of the position y and the angle ϕ is plotted in Fig. 4. The time zero is set to the point where the pulse starts. In the case of the step function (Fig. 4(a)) the domain wall oscillates to its new

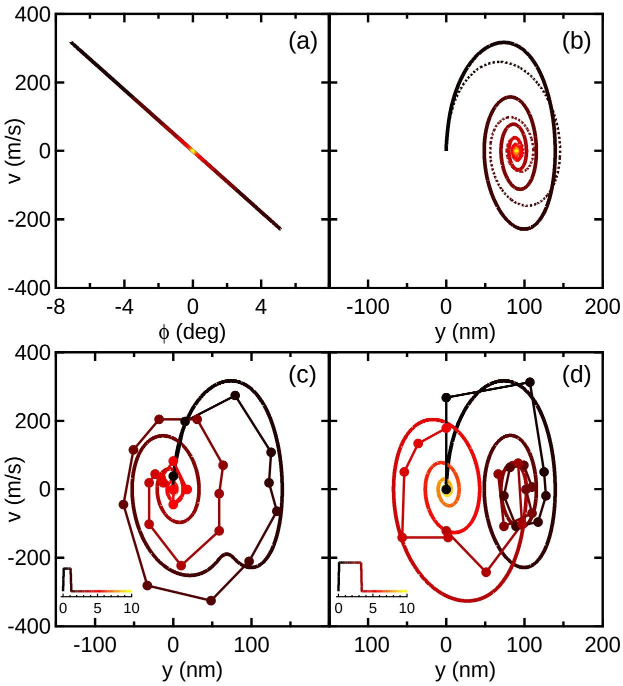

FIG. 5: (Color online) (a) Trajectory in phase space of angle ϕ and velocity v. (b)-(d) Trajectory in phase space of position Y and velocity v. The trajectories in (a) and (b) are for the step like f eld (see Fig. 4(a)). (c) and (d) also show the trajectories observed in the experiment for 1.1 ns and 3.3 ns long pulses. The lines between the dots are guides to the eye. Trajectories for the harmonic and the nonharmonic potential are the dotted and the solid lines, respectivley. Color scale is the same as in Fig. 4.

equilibrium position where the angle ϕ is zero again. For pulses the domain wall f rst oscillates towards the new equilibrium position and then oscillates back to the old equilibrium position as soon as the pulse is completed. This instantaneous reaction shows that the domain-wall mass is not directly linked to the inertial mass of a classical particle. As the equations of motion for the domain wall are differential equations of f rst order the initial velocity of the domain wall does not determine the motion of the domain wall. After integration of these equations only the initial position of the domain wall determines the temporal evolution.

One can see that the trajectory signif cantly differs due to the nonharmonic terms. Not only the position of the domain wall changes but also the out-of-plane component, i.e. the angle ϕ, can strongly differ as shown in Fig. 4(b). For a better understanding of this drastic change in ϕ it is convenient to study different phase spaces depicted in Fig. 5 for the step-like f eld. Interestingly the angle depends almost perfectly linear on the velocity with negative slope (see Fig. 5(a)) because

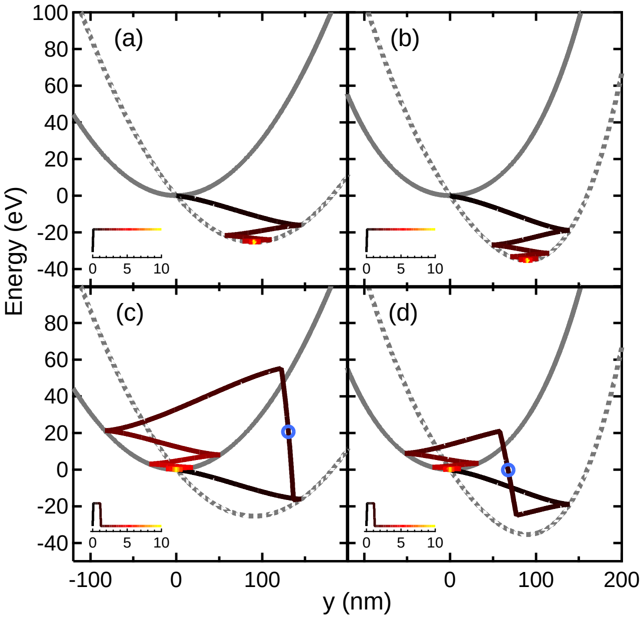

FIG. 6: (Color online) Trajectories in phase space of position and energy for the step like field (a,b) and for a field pulse of 1.1 ns (c,d). The trajectories for the harmonic potential (a,c) and the nonharmonic potential (b,d) are plotted with (dotted line) and without (solid line) applied field. The circles depict the time when the field has decreased to half of the amplitude. Color scale is the same as in Fig. 4. The insets depict the pulse profile for the first 10 ns.

the second term in Eq. (2) is orders of magnitude smaller than the first term. Then Eq. (2) simplifies to $\dot{y} = -\frac{\lambda}{\alpha\tau_d}\phi$. Consequently the trajectory in the phase space of position and velocity is inverted along the ordinate in comparison to the one in the phase space of position and angle (compare Fig. 4(a) and Fig. 5(b)). For comparison Fig. 5(c) and (d) show the trajectories observed in the experiment and calculated from the model for a 1.1 ns and a 3.3 ns field pulse.

Trajectories in phase space of position and energy are shown in Fig. 6. One can see that the domain-wall energy oscillates with its characteristic damping to the equilibrium position of the new potential well with lower potential energy due to the Zeeman contribution. For a pulse length of 1.1 ns the situation differs as the external field disappears and the energy of the domain wall returns to the original potential well. In the harmonic potential shown in Fig. 6(a) and (c) the domain-wall energy raises to a high potential energy leading to a high kinetic energy in the following. In the nonharmonic potential the domain wall is constrained sooner to the shifted equilibrium position due to the stronger restoring force. Here the domain-wall energy is much smaller after the pulse. Hence, the domain-wall velocity is smaller and consequently due to the linear dependencey its out-of-plane component.

V. CONCLUSION

We presented an analytical model which precisely describes oscillations of a magnetic domain wall in a restoring potential. Nonharmonic terms are introduced to the pinning potential to take deviations from the pure harmonic oscillator model into account. Time resolved X-ray microscopy with high spatial resolution reveals that these nonharmonic terms are necessary to describe the oscillations of a domain wall. Phase space diagrams illustrate the dynamics of the domain wall and show that the behaviour of the domain wall is strongly affected by the nonharmonic pinning potential. The damping parameter of permalloy has been determined by a direct imaging method using the domain-wall oscillation and is in excellent agreement with ferromagnetic resonance results determined for f lms.

Acknowledgments

We thank René Eiselt for collaboration in X-ray microscopy, Toru Matsuyama, Markus Bolte, Daniela Pfannkuche, and Ulrich Merkt for fruitful discussions as well as Sandra Motl for assistance with the analysis of the X-ray images and ferromagnetic resonance measurements. Financial support by the Deutsche Forschungsgemeinschaft via the SFB 668 ”Magnetism from the Single Atom to the Nanostructure” and via the Graduiertenkolleg 1286 ”Functional Metal-Semiconductor Hybrid Systems” is gratefully acknowledged. Operation of the soft X-ray microscope is funded by the Director, Offi ce of Science,of the U.S. Department of Energy under Contract No. DE-AC02-05CH11231.

---

[1] S. S. P. Parkin, M. Hayashi, and L. Thomas, Science **320**, 190 (2008).

[2] A. Drews, B. Krüger, G. Meier, S. Bohlens, L. Bocklage, T. Matsuyama, and M. Bolte, Appl. Phys. Lett. **94**, 062504 (2009).

[3] S. Bohlens, B. Krüger, A. Drews, M. Bolte, G. Meier, and D. Pfannkuche, Appl. Phys. Lett. **93**, 142508 (2008).

[4] A. A. Thiele, Phys. Rev. Lett. **30**, 230 (1973).

[5] N. L. Schryer and L. R. Walker, J. Appl. Phys. **45**, 5406 (1974).

[6] B. Krüger, D. Pfannkuche, M. Bolte, G. Meier, and U. Merkt, Phys. Rev. B **75**, 054421 (2007).

[7] B. Krüger, A. Drews, M. Bolte, U. Merkt, D. Pfannkuche, and G. Meier, Phys. Rev. B **76**, 224426 (2007).

[8] M. Kläui, P.-O. Jubert, R. Allenspach, A. Bischof, J. A. C. Bland, G. Faini, U. Rüdiger, C. A. F. Vaz, L. Vila, and C. Vouille, Phys. Rev. Lett. **95**, 026601 (2005).

[9] M. Hayashi, L. Thomas, C. Rettner, R. Moriya, and S. S. P. Parkin, Nat. Phys. **3**, 21 (2007).

[10] G. Meier, M. Bolte, R. Eiselt, B. Krüger, D.-H. Kim, and P. Fischer, Phys. Rev. Lett. **98**, 187202 (2007).

[11] M. Bolte, G. Meier, B. Krüger, A. Drews, R. Eiselt, L. Bocklage, S. Bohlens, T. Tyliszczak, A. Vansteenkiste, B. Van Waeyenberge, et al., Phys. Rev. Lett. **100**, 176601 (2008).

[12] L. Bocklage, B. Krüger, R. Eiselt, M. Bolte, P. Fischer, and G. Meier, Phys. Rev. B **78**, 180405(R) (2008).

[13] O. Boulle, L. Heyne, J. Rhensius, M. Kläui, U. Rüdiger, L. Joly, L. L. Guyader, F. Nolting, L. J. Heyderman, G. Malinowski, et al., J. Appl. Phys. **105**, 07C106 (2009).

[14] W. Chao, B. D. Harteneck, J. A. Liddle, E. H. Anderson, and D. T. Attwood, Nature **435**, 1210 (2005).

[15] A. Puzic, B. Van Waeyenberge, K. W. Chou, P. Fischer, T. Tyliszczak, K. Rott, H. Brückl, G. Reiss, I. Neudecker, T. Haug, et al., J. Appl. Phys. **97**, 10E704 (2005).

[16] S. Ingvarsson, L. Ritchie, X. Y. Liu, G. Xiao, J. C. Slonczewski, P. L. Trouilloud, , and R. H. Koch, Phys. Rev. B **66**, 214416 (2002).

[17] M. Bailleul, D. Olligs, and C. Fermon, Appl. Phys. Lett. **83**, 972 (2003).

[18] D. J. Twisselmann and R. D. McMichael, J. Appl. Phys. **93**, 6903 (2003).

[19] S. Tamaru, J. A. Bain, R. J. M. van de Veerdonk, T. M. Crawford, M. Covington, and M. H. Kryder, Phys. Rev. B **70**, 104416 (2004).

[20] M. L. Schneider, T. Gerrits, A. B. Kos, and T. J. Silva, Appl. Phys. Lett. **87**, 072509 (2005).

[21] S. S. Kalarickal, P. Krivosik, M. Wu, C. E. Patton, M. L. Schneider, P. Kabos, T. J. Silva, and J. P. Nibarger, J. Appl. Phys. **99**, 093909 (2006).

[22] W. Döring, Z. Naturforsch. **3a**, 373 (1948).

[23] D. Bedau, M. Kläui, M. T. Hua, S. Krzyk, U. Rüdiger, G. Faini, and L. Vila, Phys. Rev. Lett. **101**, 256602 (2008).

[24] C. Chen, F. Setter, Y. Ma, and S. Modesti, Phys. Rev. B **42**, 7262 (1990).

[25] We use $\alpha = 0.01$ for permalloy.

[26] J. Podbielski, F. Giesen, and D. Grundler, Phys. Rev. Lett. **96**, 167207 (2006).